Construction of a pathological model of skin lesions in acute herpes zoster virus infection and its molecular mechanism

Hao Zhou[1] · Zheng Ye[2] · Zhao Gao[1] · Chengxi Xi[1] · Jinxia Yin[1] · Yanjun Sun[1] · Bo Sun[3]

Abstract

Varicella-zoster virus (VZV), a common pathogen with humans as the sole host, causes primary infection and undergoes a latent period in sensory ganglia. The recurrence of VZV is often accompanied by severe neuralgia in skin tissue, which has a serious impact on the life of patients. During the acute infection of VZV, there are few related studies on the pathophysiological mechanism of skin tissue. In this study, transcriptome sequencing data from the acute response period within 2 days of VZV antigen stimulation of the skin were used to explore a model of the trajectory of skin tissue changes during VZV infection. It was found that early VZV antigen stimulation caused activation of mainly natural immune-related signaling pathways, while in the late phase activation of mainly active immune-related signaling pathways. JAK-STAT, NFκB, and TNFα signaling pathways are gradually activated with the progression of infection, while Hypoxia is progressively inhibited. In addition, we found that dendritic cell-mediated immune responses play a dominant role in the lesion damage caused by VZV antigen stimulation of the skin. This study provides a theoretical basis for the study of the molecular mechanisms of skin lesions during acute VZV infection.

Keywords Varicella-zoster virus · Skin lesion · Pseudo-time · Bioinformatic · Molecular mechanism

Introduction

Herpes zoster (HZ) is the clinical manifestation of the reactivation of varicella zoster virus (VZV) (Oxman 2000). Following infection, VZV is dormant in sensory neurons(Sadzot-Delvaux et al. 1990). When the immune system is compromised or immune function is reduced, the

Hao Zhou and Zheng Ye contributed equally to this work and share first authorship.

✉ Yanjun Sun
1330148022@qq.com

✉ Bo Sun
sunbo@seu.edu.cn

1 Department of Anesthesia Surgery and Pain Management, Southeast University Zhongda Hospital, Nanjing 210009, China

2 Institute of Computational Science and Technology, Guangzhou University, Nanjing 510006, China

3 State Key Laboratory of Digital Medical Engineering, School of Biological Science & Medical Engineering, Southeast University, Nanjing 210096, China

virus can be reactivated, leading to shingles(Stankus et al. 2000). VZV is a member of the herpes virus with a diameter of about 150–200 nm and a core of double-stranded DNA (You et al. 2017). Viruses have three-dimensionally symmetrical capsids. Outside the capsid is a spherical envelope composed of lipids and proteins, and only the enveloped virus is infectious(Sun et al. 2020). There are 6–8 glycoproteins on the viral film. The viral glycoproteins gp1, gp2 and gp3 all induce neutralising antibodies in the body, with gp1 being the main antigen of the virus and the main source for the preparation of viral vaccines(Vafai et al. 1984). VZV is able to multiply in the nuclei of human embryonic fibroblasts and epithelial cells and produce focal cytopathies. Humans are the only known host in nature (Balfour 1988); (Yamanishi et al. 1980). After primary infection with VZV, the virus ascends through the sensory nerves and forms an incisional infection in one or more of the spinal dorsal root ganglia and trigeminal ganglia (Gershon and Gershon 2013), (Hyman et al. 1983). Despite the widespread incidence of herpes zoster virus and the large number of potential infections, yet the molecular mechanisms underlying changes in skin samples during acute infection remain unclear.

In this study, we explored the molecular mechanisms of local skin lesions caused by acute VZV infection and changes in the microenvironment of skin tissues using transcriptome sequencing data obtained from VZV antigen infection of human skin. The study reveals the early and late stages of acute VZV-induced skin lesions, reveals the molecular biology and cell biology mechanisms, and provides a theoretical basis for the prevention and treatment of VZV-induced skin lesions. The specific process of the research is shown in Fig. 1.

Methods

Data sources

The data used in this study, GSE130633(Chambers et al. 2021), was derived from the GEO database(Barrett et al. 2012). The samples came from human patient biopsies. The cohort contains high throughput sequencing data from 126 skin lesions caused by VZV antigen stimulation. These samples contained 30 normal skin samples, 30 samples after 6 h saline injections, 32 samples after 6 h VZV antigen treatment and 34 samples after 2 days VZV antigen treatment.

Data processing flow

We use "Seurat 4.0" R package(Ye et al. 2022), (Butler et al. 2018) to construct Seurat objects for 126 samples. The samples are then preprocessed by "SCTransform" function (Hafemeister and Satija 2019). After obtaining a normalized

expression profile matrix, linear dimensionality reduction was performed using "RunPCA" function to identify the main top 30 principal components. The distance between samples was calculated using "FindNeighbors" function (ndims = 1:30), and nonlinear dimensionality reduction was carried out on the samples using "RunUMAP" function (ndims = 30). For the differential expression analysis, the One vs. Others strategy was utilized to identify differentially expressed genes in different treatment groups using the "FindAllMarker" (wilcoxon test) function. Genes meeting the screening criteria of adj.$p < 0.01$ and abs (avg_log2FC) > 1 were considered as differentially expressed genes.

Functional enrichment analysis

Gene sets were subjected to functional enrichment analysis using "clusterprofileR" R package (Wu et al. 2021). First, overexpression analysis was performed on the differentially expressed genes of different treatment groups. Second, GSEA was performed on the eigengenes of the PC1 axis and PC2 axis. Gene sets of GO (G.O.C.J 2004) and KEGG (Kanehisa and Goto 2000) were used for overexpression analysis. Whereas GSEA (Reimand et al. 2019) uses the MSIGDB C2 KEGG (Liberzon et al. 2011) gene set.

ssGSEA

To further compare the differences in signaling pathways in each sample, the ssGSEA (Hänzelmann et al. 2013) algorithm in "GSVA" R package was used to evaluate

Fig. 1 Work flow
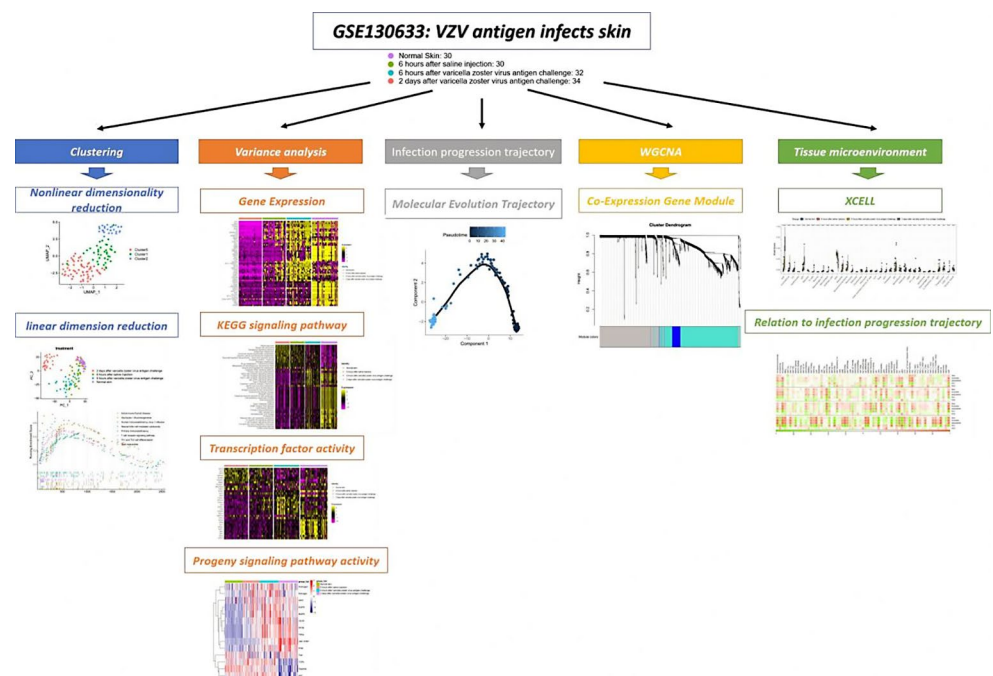
the enrichment of signaling pathways in the MSigDB C2 KEGG gene set in 126 samples. Differences in signaling pathways between treatment groups were found using the "FindAllMarker" (wilcoxon test) function.

Transcription factor activity analysis

"DoRothea" R package (Holland et al. 2020) was used to assess the transcription factor activity of 126 samples. First, the transcription factor regulatory networks with confidences of A, B, C were selected from the "doRothea_hs" function (DoRothEA is a gene set containing transcription factors that interact with their targets. Different types of interaction evidence such as interaction inference from gene expression. The trustworthiness of the interaction between TF and target was classified into five levels (A–E) according to the amount of supporting evidence, with A being the most credible and E being the low trustworthiness. In this study, grades A, B, and C were selected at medium confidence). The transcription factor activity matrix was then obtained by assessing the transcription factor activity of 126 samples using the "run_viper" function. The information was integrated into the Seurat object by constructing an Assay object. The "FindAllMarker" (wilcoxon test) function was used to find differences in transcription factor activity across treatment groups.

Signal pathway activity analysis

"PROGENy" R package (Schubert et al. 2018) utilizes a vast collection of publicly available signaling perturbation experiments to identify a shared set of pathway responsive genes for both human and mouse. These genes, in combination with any statistical approach, can be employed to predict pathway activities from either bulk or single-cell transcriptomic data. In our study, we used the R package "decoupleR" (Badia-i-Mompel et al. 2022) to evaluate the activity of 14 common signaling pathways in 126 skin samples. Initially, we constructed a model using the top 500 genes with the "get_progeny" function. Subsequently, we assessed the weights of the 14 signaling pathways in the 126 samples using the average weight algorithm ("run_wmean" function).

Pseudo-time series analysis

After the skin is stimulated by VZV antigen, it will experience a series of pathological changes successively. "Monocle" R package (Perešíni et al. 2015) was used to construct pseudo-temporal trajectories of skin samples. First convert the Seurat object to a CDS object through the "as.CellDataSet" function. Next, we use the differentially expressed genes to reduce the dimension of the sample ("DDRTree" R package) to construct the dynamic change trajectory of the sample. To find the main regulatory genes driving skin changes, we used the differentialGeneTest function (fullModelFormulaStr = " ~ sm.ns (Pseudo-time)") to analyze the samples. We screened the top 200 genes for clustering and visualization based on the ranking of q.values to find gene modules that regulate changes in skin samples.

Tissue microenvironment analysis

We utilized "XCELL" R package (Aran et al. 2017) to assess the scores of 64 cell types in 126 samples. As part of the data processing, the transcriptome data underwent normalization through a logarithmic transformation ($\log2$ (TPM + 1). Default parameters were applied in XCELL, and the results of the evaluation were recorded in Appendix 1.

Weighted gene co-expression network analysis (WGCNA)

Gene co-expression regulatory modules associated with clinical traits can be found by "WGCNA" R package (Langfelder and Horvath 2008), which has been widely used in the transcriptomic and proteomic fields. Firstly, we performed voom normalization of expression profile data from 126 skin samples by the R package "limma". The normalised expression profile matrix was then used to construct a gene co-expression regulatory network using the R package "WGCNA". We screened genes with standard deviation greater than 1 for subsequent co-expression module analysis. To make the modules conform to the scale-free network characteristics, we suspended a soft threshold of 10 and fused genes with distance less than 0.25 to form the co-expression modules. We eventually obtained 2 co-expression modules (blue and turquoise). We calculated the relationship between the principal components (ME) of the two modules and the different treatment groups of the skin.

Statistics

R version 4.1 was used for analysis of data and plotting of images. the R package "pscych" (Revelle and Revelle 2015) was used for correlation analysis (spearman) and corrplot for plotting correlation heat maps. the R packages "ggplot2", "ggpubr" (Kassambara and Kassambara 2020) were used for statistical plotting. Comparisons between multiple groups were performed using kruskal-wallis.

Results

Transcriptome distribution characteristics of VZV antigen-stimulated skin samples

Three clusters were obtained by non-linear dimensionality reduction (UMAP) and unsupervised clustering (Louvain) of 126 skin samples (cluster0: 61 samples, cluster1: 38 samples, cluster2: 27 samples; Fig. 2A and B). We performed chi-square tests on the samples from each of the four treatments within the three clusters. The results revealed that in cluster 0, 49% of the samples were Normal skin, 31% were from 6 h after saline injection, 8% were from 6 h after VZV antigen challenge, and 11% were from 2 days after VZV antigen challenge. For cluster 1, 68% were from 6 h after VZV antigen challenge, 29% were from 6 h after saline injection, and only 3% were from 2 days after VZV antigen

challenge. In cluster 2, 96% were from 2 days after VZV antigen challenge, and only 4% were from 6 h after VZV antigen challenge (Fig. 2C).

This result could reflect the severity of VZV antigen irritation of the skin as cluster2 > cluster1 > cluster0. Further exploring the expression profile characteristics of the different treatment groups, we can observe on the PCA 2D scatter plot that 2 days after VZV antigen challenge and Normal Skin are more closely distributed on PC2, while the 6 h after saline injection group and 6 h after VZV antigen challenge group are mainly distributed on the negative axis of PC2. Furthermore, we can clearly observe that the temporal axis of VZV antigen infection is distributed along PC1 (Fig. 2D). We performed GSEA (MSIGDB KEGG gene set) based on the ranking of the contribution of genes to the PC axis. The results showed that the genes contributing positively to the PC1 axis were mainly enriched in AMPK signaling pathway,

Fig. 2 Transcriptome dynamics after VZV antigen stimulation of the skin. (**A**) The Louvain cluster can classify 126 skin samples into three categories (cluster0, cluster1, cluster2). (**B**) Distribution of the four treatment groups in a UMAP two-dimensional scatter plot. (**C**) Correlation of the Louvian cluster with the distribution of the 4 treatment groups. A chi-square test was used to compare differences between the subgroups. (**D**) Distribution of 126 skin samples in linear reduced dimensional (PCA) space. It can be observed from the figure that the PC1 axis mainly determines viral infection and the PC2 axis mainly determines wound healing. (**E**) GSEA results for genes contributing positively to the PC1 axis. (**F**) GSEA results for genes contributing negatively to the PC1 axis. (**G**) GSEA results for genes contributing positively to the PC2 axis. (**H**) GSEA results for genes contributing negatively to the PC2 axis
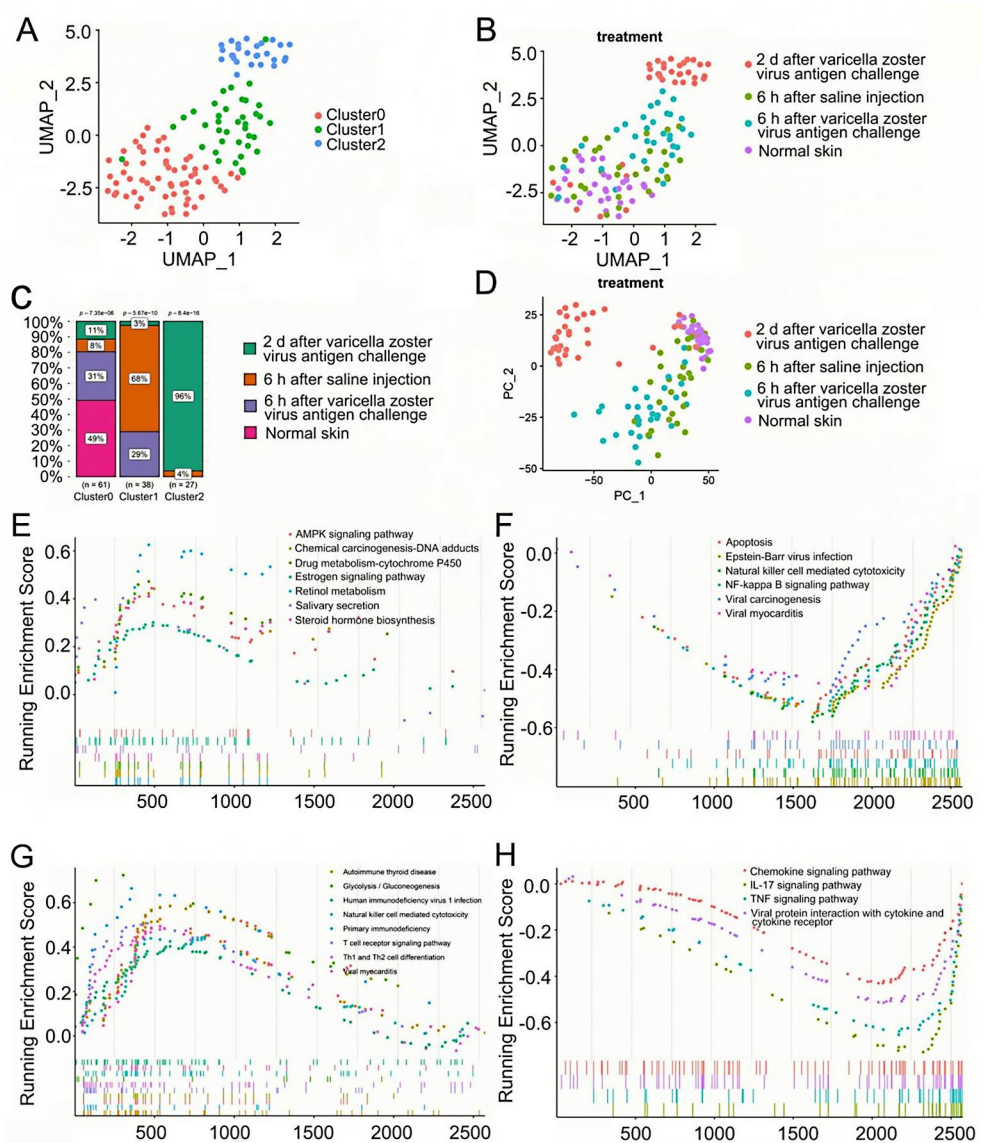
Chemical carcinogenesis-DNA adducts, Drug metabolism-cytochrome P450, Estrogen signaling pathway, Retinol metabolism, Salivary secretion, Steroid hormone biosynthesis and other signaling pathways (Fig. 2E). Genes contributing negatively to the PC1 axis were mainly enriched in Apoptosis, Epstein-Barr virus infection, Naturall killer cell mediated cytotoxicity, NF-kappa B signaling pathway, Viral carcinogenesis, Viral myocarditis and other signaling pathways (Fig. 2F). Genes that positively contribute to the PC2 axis are primarily enriched in Autoimmune thyroid disease, Glycolysis/Gluconeogenesis, Human immunodeficiency virus1 infection, Natural killer cell mediated cytotoxicity, Primary immunodeficiency, T cell receptor signaling pathway, Th1 and Th2 cell differentiation, and Viral myocarditis (Fig. 2G). Conversely, genes that negatively contribute to the PC2 axis are mainly enriched in the Chemokine signaling pathway, IL-17 signaling pathway, TNF signaling pathway, Viral protein interaction with cytokine and cytokine receptor, and other signaling pathways (Fig. 2H). The PC2 axis mainly reflects the stress response of the skin to the wound.

Differences in gene expression signatures of VZV antigen-stimulated skin

We compared the expression profile characteristics of skin samples from four different treatment groups from three different perspectives. First, we performed differential expression analysis of the expression profiles of the four subgroups (One vs. Others strategy) and performed functional enrichment analysis (GO) of the upregulated genes in each treatment group by clusterprofileR (Fig. 3A, Fig. S1). We found that postsynapic-related signaling pathways were significantly activated in the 6 h after saline injection group. The cytokine and chemokine-related signaling pathways were significantly activated in the VZV antigen challenge group after 6 h. Immune-related signaling pathways were significantly activated in the VZV antigen challenge group after 2 days.

Further, we assessed the activity of 186 KEGG gene sets from 126 skin samples using ssGSEA. The results showed that innate immunity and active immunity-related pathways were activated, and cellular metabolism-related pathways were inhibited in the VZV antigen challenge group after 6 h and in the VZV antigen challenge group after 2 days (Fig. 3B). Innate immunity related pathways including Cytosolic DNA-sensing pathway, NOD-like receptor signaling pathway, Toll-like receptor signaling pathway, RIG-I-like receptor sighalng patway, jak-STAT signaling pathway, Type ll diabetes mellitus, Cytokine-cytokine receptor interaction. Active immunity related pathways including Systemic lupus erythematosus, Antigen processing and

presentation, Autoimmune thyroid disease, Allograft rejection, Intestinal immune network for lgA production, Cell adhesion molecules(CAMs), Viral myocarditis, Asthma, Type l diabetes mellitus, Graft-versus-host disease, Leishmania infection, Primary immunodeficiency, ABC transporters, Hematopoietic cell lineage, Proteasome, Natural killer cell mediated cytotoxicity, Fc epsilon Rl signaling pathway, T cell receptor signaling pathway, Complement and coagulation cascades, Chemokine signaling pathway, Folate biosynthesis. Cellular metabolism-related pathways including Melanogenesis, Basal cell carcinoma, Hedgehog signaling pathway, Butanoate metabolism, Proximal tubule bicarbonate reclamation, Glycine, serine and threonine metabolism, Glycosphingolipid biosynthesis-lacto and neo-lacto series, Circadian rhythm-mammal, Nitrogen metabolism, Drug metabolism-cytochrome P450, Metabolism of xenobiotics by cytochrome P450, Taurine and hypotaurine metabolism.

Further, we compared the differences in transcription factor activity. BCL6, GLI2, ATF3, KMT2A, NFKB2, TFAP2C were significantly activated in the Normal skin group, and these genes are involved in the regulation of DNA methylation. In the 6 h after VZV antigen challenge group, transcription factors such as FOXL2, NR1H2, FOSL2, JUN were significantly activated, and these genes are involved in the Th17 cell differentiation and Positive regulation of miRNA transcription. The transcription factors RFX5, SPIB, LYL1, TBX21 were significantly activated in the 2 days after VZV antigen challenge group, and these genes are involved in the Human T-cell leukemia virus 1 infection and Hepatitis B (Fig. 3C).

Ultimately, we compared the activation levels of 14 prevalent signaling pathways in 126 skin samples. Our findings indicated a progressive increase in the activity of JAK-STAT, NF-κB, TNF-α, VEGF, and PI3K signaling pathways with the advancement of skin infection, while the activity of the Hypoxia signaling pathway decreased progressively. Additionally, we observed a notable reduction in the activities of the p53 and TGF-β signaling pathways in the group following VZV antigen challenge after 2 days (Fig. 3D and E).

Changes in the tissue microenvironment during skin stimulation by the VZV antigen

We used XCELL to assess the tissue infiltration scores of 64 cell types and 3 integrated scores from 126 skin samples. We found that most of the immune cells (DC cells, B cells, T cells, Macrophage, etc.) scores increased with disease progression, while some stromal cells (Keratinocytes, Myocytes, HSC, Chondrocytes, etc.) scores decreased (Fig. 4).
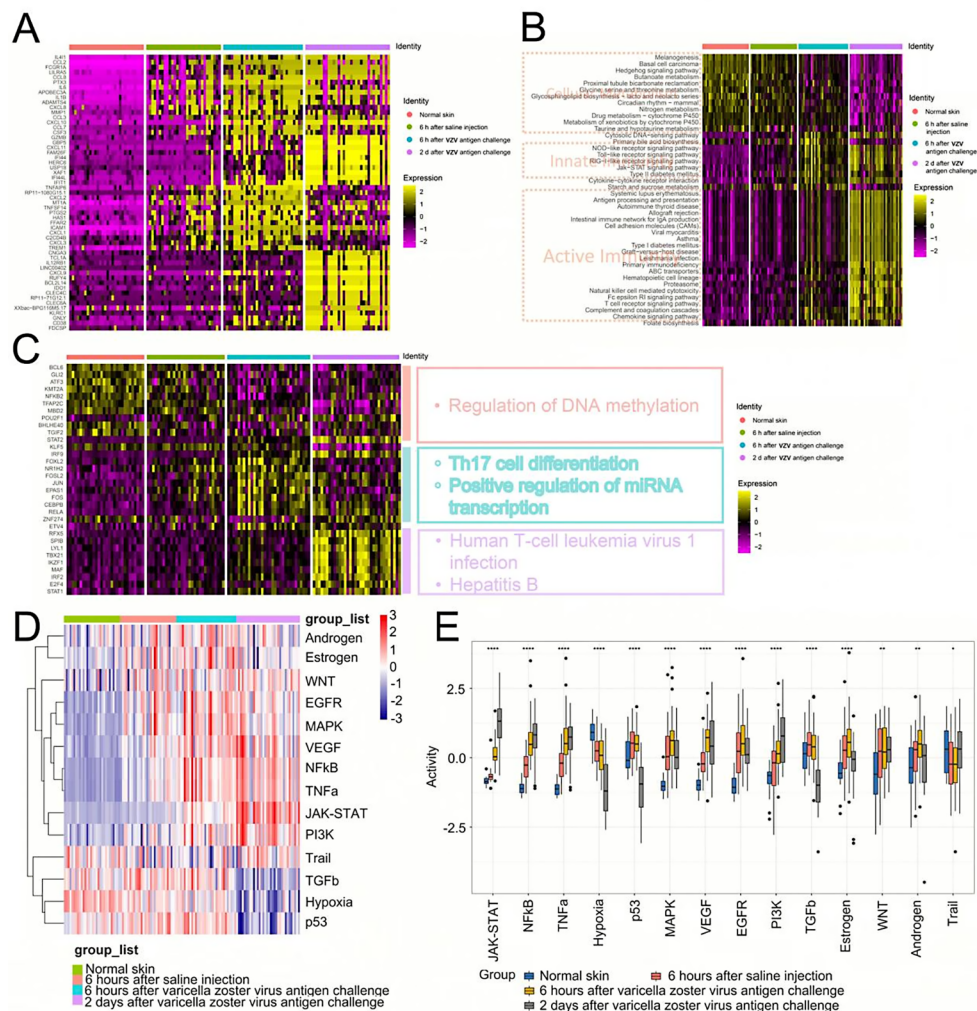
Fig. 3 Multidimensional comparison of differences in skin samples from the four treatment groups. (**A**) Transcriptome differences. (**B**) Differences in KEGG signaling pathway enrichment scores. From the figure, it can be seen that the Normal skin, 6 h after saline injection group had significant activation of cellular metabolism related signaling pathways. The VZV antigen challenge group showed significant activation of Innate Immunity related signaling pathway. 2 days after VZV antigen challenge group showed significant activation of Active Immunity. (**C**) Differences in transcription factor activity. normal skin, 6 h after saline injection group showed high expression of transcription factors mainly involved in Regulation of DNA methylation. 6 h after VZV antigen challenge group showed high expression of transcription factors mainly in Th17 cell differentiation. The transcription factors in the 6 h after VZV antigen challenge group were mainly enriched in Th17 cell differentiation, Positive regulation of miRNA transcription signaling pathway. The transcription factors that were highly expressed in the 2 days after VZV antigen challenge group were mainly enriched in the Human T-cell leukemia virus 1 infection, Hepatitis B signaling pathway. (**D**, **E**) Results of signaling pathway activity analysis using the Progeny algorithm

The pseudo-chronological progression model of VZV antigen-infected skin

To explore the progression characteristics of VZV antigen-stimulated skin, we constructed a disease progression model using monocle. We found that VZV antigen-infected skin progresses through Normal skin, 6 h after saline injection, 6 h after VZV antigen challenge, and finally to 2 days after VZV antigen challenge (Fig. 5A and B). The CXCL10, CXCL11, GBP5, GZMB, IL1B, IRG1 were all elevated with Pseudo-time (Fig. 5C). This implies that these

genes are gradually upregulated in the process of cell state changes and are likely to regulate the deterioration or progression of the disease state. We screened the top 200 genes associated with Pseudo-time (rank by q.value). These 200 genes could be clustered into 3 clusters (cluster1, cluster2, cluster3; Fig. 5D), with cluster 3 having the highest correlation with disease progression. Figure 5E shows that cluster 2 is mainly enriched on the T cell receptor signaling pathway, Cytokine-cytokine receptor interaction, Hematopoietic cell lineage, Th17 cell differentiation, Cell adhesion molecules, Th1 and Th2 cell differentiation, Chemokine signaling pathway, Primary immunodeficiency, Natural killer
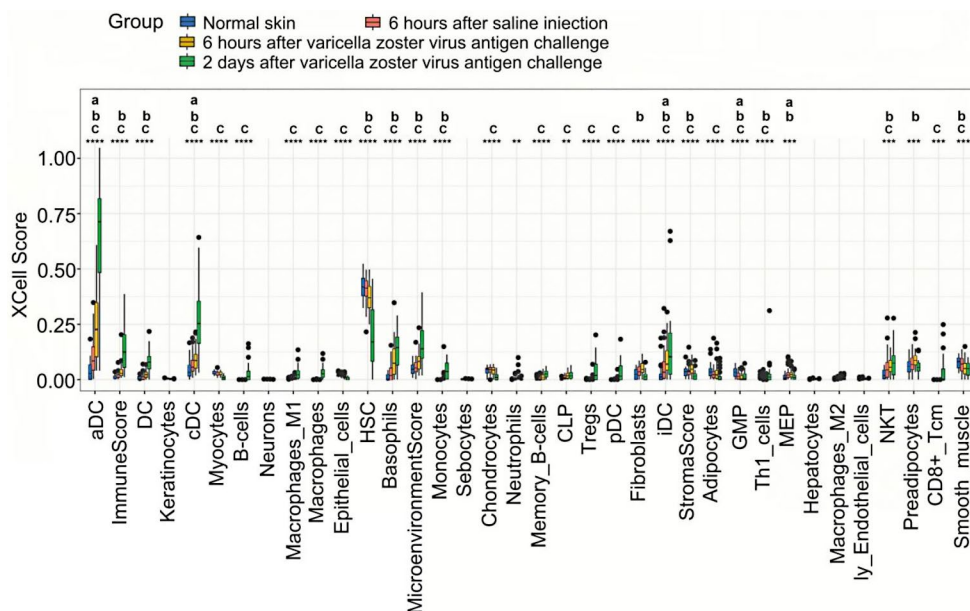
Fig. 4 Comparison of the scores of cells obtained by the XCELL algorithm in the four treatment groups. It can be seen that immune-related cells (DCs, B-cells, Macrophages, Basophils, etc.) gradually increase with VZV antigen infection of the skin, while stromal cells (Neurons, Epithelial cells, HSC, Smooth muscle) gradually decrease. The * represents the significance of the contrast between the four treat-ment groups; **$P < 0.01$; ***$P < 0.001$; ****$P < 0.0001$. The a represents the significance of the contrast between normal skin and 6 h after saline iniection. The b represents the significance of the contrast between normal skin and 6 h after varicela zoster virus antigen challenge. The c represents the significance of the contrast between normal skin and 2 days after varicela zoster virus antigen challenge

cell mediated cytotoxicity, PD-L1 expression and PD-1 checkpoint pathway in cancer. Figure 5 F shows that cluster 1 is mainly enriched on the Cytokine-cytokine receptor interaction, Viral protein interaction with cytokine and cytokine receptor, Chemokine signaling pathway, Rheumatoid arthritis, IL-17 signaling pathway, Chagas disease, NF-kappa B signaling pathway, Toll-like receptor signaling pathway, Malaria, Pertussis. Figure 5G shows that cluster 1 is mainly enriched on the Osteoclast differentiation, Cytokine-cytokine receptor interaction, Viral protein interaction with cytokine and cytokine receptor, Measles, Chemokine signaling pathway, B cell receptor signaling pathway, lL-17 signaling pathway, Staphylococcus aureus infection, Hematopoietic cell lineage.

Gene expression regulation during VZV antigen-stimulated skin progression in relation to the tissue microenvironment

We first analyzed 126 skin samples with WGCNA and found two co-expressed regulatory modules (blue module and turquoise module; Fig. 6A, B, C). Among them, the Turquoise module was highly correlated with virus infection (6 h after VZV antigen challenge: $R = 0.72$, $p < 0.001$; 2 days VZV antigen challenge: $R = 0.74$, $p < 0.001$; Fig. 6D). Functional enrichment analysis and PPI regulatory network analysis were performed on the hub genes (MM > 0.7) in the module

using Metascape, respectively. The blue module hub genes (72) are mainly involved in the Leukocyte migration signaling pathway, and the core genes of its PPI regulatory network are mainly involved in the Interleukin-10 signaling pathway (IL6, CXCL8, CXCL1, IL1B, CCL2, CXCL2; Fig. 6E, F). Turquoise module hub genes (457) are mainly involved in the Cell activation signaling pathway, and the core genes of its PPI regulatory network are mainly involved in Cytokine Signaling in immune system, TCR pathway and other signaling pathways (Fig. 6G, H). The results showed that these key genes of VZV antigen-stimulated skin progression were closely related to the tissue microenvironment.

Next, to explore the relationship between molecular biological mechanisms and cellular infiltration of the tissue microenvironment during the progression of VZV antigen infection of the skin, we compared 64 cells in four treatment groups with co-expression modules (blue and turquoise), Pseudo-time, PC1, PC2 using Spearman's correlation coefficients (Fig. 7). We found that DC was positively correlated with blue, turquoise, and Pseudo-time and negatively correlated with PC1 in all four treatment groups. Basophils in VZV antigen-stimulated skin correlated positively with blue, turquoise, and Pseudo-time and negatively with PC1; CD4 + memory T cells and CD4 + naive T cells, CD4 + Tem, CD8 + Tcm correlated positively with blue, turquoise, Endothelial cells and Epithelial cells were negatively correlated with blue, turquoise, Pseudo-time and

Fig. 5 Modeling the differentiation trajectory of VZV antigen-stimulated skin. (**A**) The differentiation trajectory of VZV antigen-stimulated skin was constructed from transcriptomic data of 126 skin samples (P value < 0.05). (**B**) Distribution of the four different treatment groups on the two-dimensional scatter plot obtained by the DDRTree algorithm. From the plot, we can find that the Normal skin group is at the initial stage of differentiation, while the 2 days after VZV antigen challenge group is at the end of differentiation (P value < 0.05). (**C**) CXCL10, CXCL11, GBP5, GZMB, IL1B, and IRG1 increased progressively with the progression of Pseudo-time (P value < 0.05; q value < 0.05). (**D**) The major regulatory genes (top200) that drive VZV antigen-stimulated skin differentiation. These 200 genes can be divided into 3 clusters. (**E**) Gene set enrichment results for the cluster2 gene module. (**F**) Gene set enrichment results for the cluster1 gene module. (**G**) Gene set enrichment results for the cluster3 gene module. The gene set used for gene enrichment is the KEGG gene sets
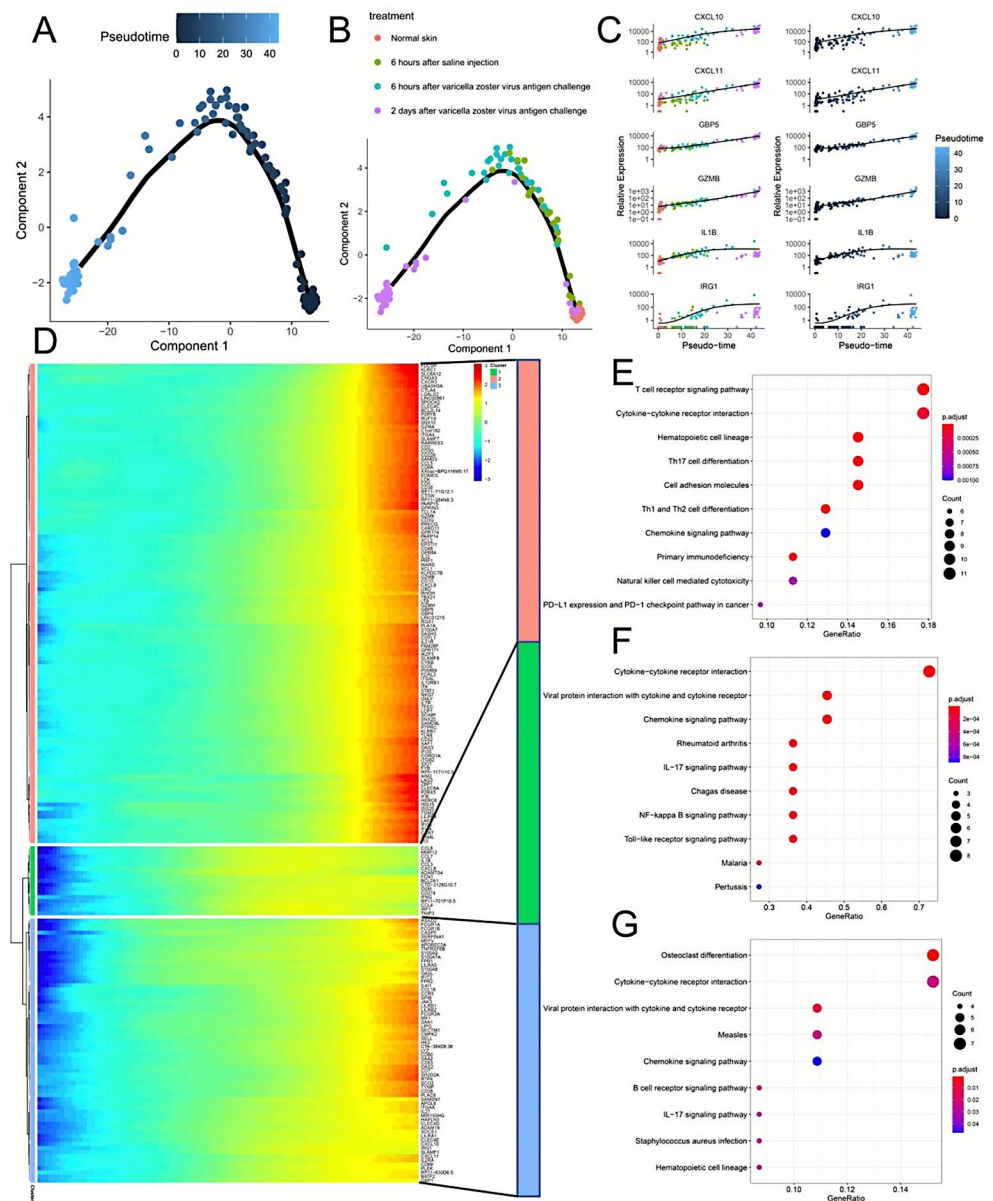
positively correlated with PC1. Macrophage M1 was negatively correlated with blue, turquoise, and Pseudo-time and positively correlated with PC1 in the VZV antigen-infected group, whereas Macrophage M2 was positively correlated with turquoise, Pseudo-time and negatively correlated with PC1 in the Normal skin group. Notably, Fibroblast was positively correlated with blue, turquoise, and Pseudo-time and negatively correlated with PC1 in the 6 h after saline injection group, while the opposite was true in the 2 days after VZV antigen challenge group. Neurons in the 6 h after saline injection, 6 h after VZV antigen challenge group were significantly negatively correlated with blue, turquoise, Pseudo-time and positively correlated with PC1. Neutrophils were only positively correlated with blue, turquoise, Pseudo-time and negatively correlated with PC1 and PC2

in the 6 h after saline injection and 6 h after VZV antigen challenge groups. Th1 cells and Tregs were only positively correlated with blue, turquoise, Pseudo-time and negatively correlated with PC1 in the 2 days VZV antigen challenge group. Overall, ImmuneScore showed a significant increase in cellular composition and a significant decrease in StromaScore following VZV antigen stimulation of the skin. This reflects the typical characteristics of skin following VZV antigen stimulation.

Fig. 6 WGCNA results for 126 skin samples. (**A**, **B**) Optimal soft thresholds were chosen to make the gene expression network conform to a scale-free distribution. (**C**) Finally, 2 co-expression modules were obtained. (**D**) Relationship between the blue and turquoise modules and the four treatment groups. The highest correlation of the turquoise module with VZV antigen stimulation can be found in the figure ($R > 0.7$, $P < 0.001$). (**E**) Functional enrichment analysis of the hub genes of the blue module (Module Membership > 0.7). (**F**) Results of the core regulatory modules and functional enrichment analysis of the PPI network constructed by the blue module of hub genes. (**G**) Functional enrichment analysis of the turquoise module's hub genes (Module Membership > 0.7). (**H**) Results of core regulatory modules and functional enrichment analysis of PPI networks constructed from the hub genes of the turquoise module
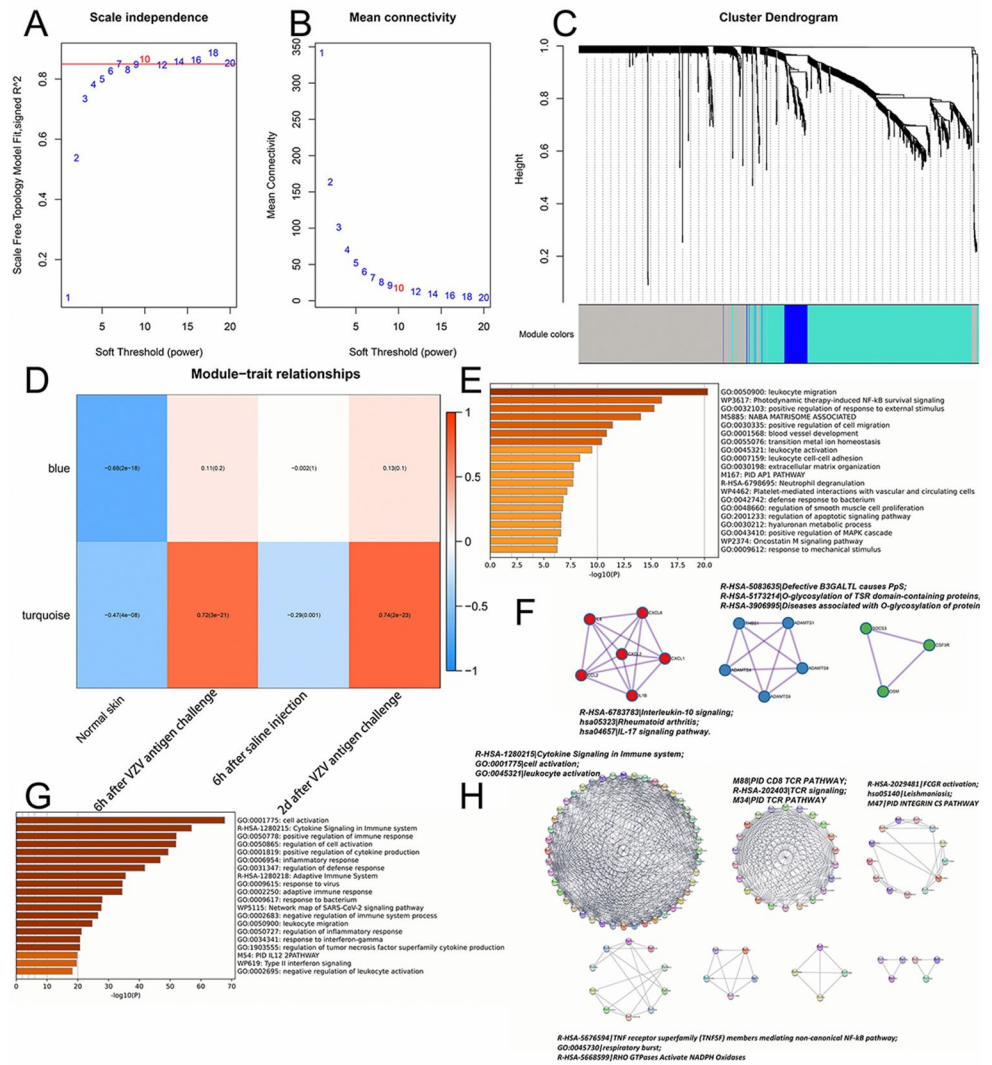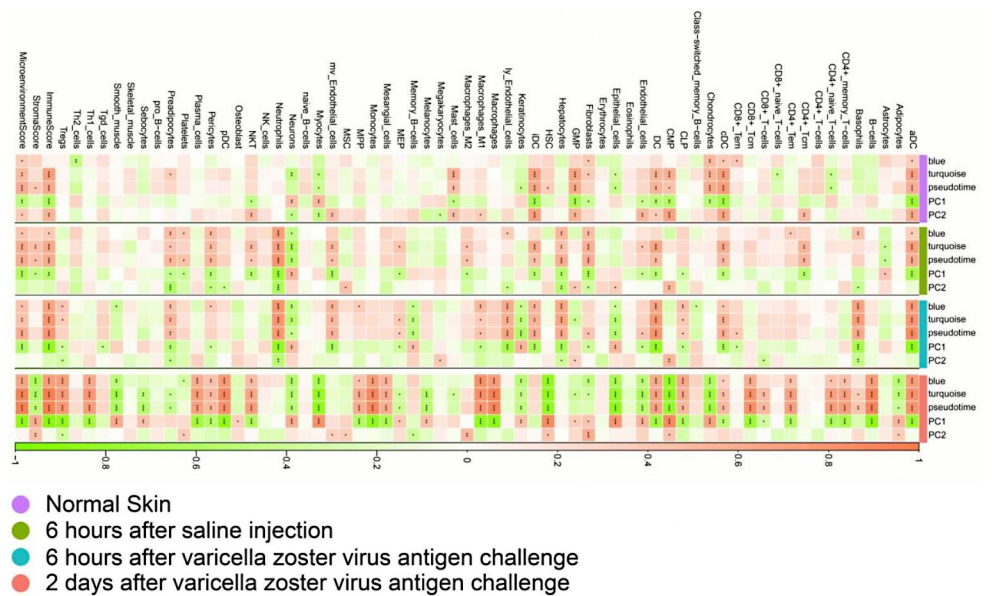

Fig. 7 Correlation analysis of 64 immune cells and three composite indices with blue, turquoise, PC1, PC2, Pseudotime in the four treatment groups (Wilcoxon test). *** $P < 0.001$, ** $P < 0.01$, * $P < 0.05$

Discussion

Herpes zoster (HZ), commonly known as shingles, occurs due to the reactivation of the varicella-zoster virus (VZV), which remains dormant in the spinal cord and cranial sensory ganglia following the initial childhood infection (Gershon and Gershon 2013). The characteristic presentation of herpes zoster includes a painful, reddish, maculopapular rash that forms fluid-filled lesions before crusting over (Schellack 2011). Reactivation of VZV leading to HZ or shingles is often associated with age-related decline in immunity or immunosuppressive conditions (Gershon et al. 2010). HZ is distinguished by a painful or itchy blistering rash, typically occurring on one side of the body. While the associated pain can persist, the average duration of the HZ rash is 7 to 10 days, and the skin typically heals completely within approximately 2 to 4 weeks (Gater et al. 2014). Despite the widespread occurrence of HZ, the pathogenic mechanisms of skin infections caused by VZV are not extensively studied. This study specifically examines the cellular and molecular processes underlying changes in skin tissue within 2 days of VZV antigen stimulation.

We firstly performed dimensionality-reduced clustering on the transcriptomes of 126 skin samples and found that the skin tissues of the four treatment groups had obvious heterogeneity and exhibited typical time-series features on the UMAP 2D scatterplot. To this end, we explored the temporalization characteristics of the samples using proposed temporal sequence analysis to find disease progression trajectories following VZV antigen stimulation of the skin within 2 days. The use of time-series analysis to model cell differentiation trajectories at the single-cell level has been widely used in single-cell transcriptomics. However, such studies at the bulk RNA level are still relatively rare. As the early infection process of the skin to VZV is distinctly chronological, this analytical approach can conveniently help us to unravel the main molecular biological regulatory mechanisms driving the progression of skin infection. Using monocle, we identified the main regulatory factors driving the skin's response to VZV antigen stimulation. We found that inflammation and activation of antiviral-related signaling pathways are typical features of VZV-infected skin. This result is consistent with the previous findings(Arvin et al. 2010).

We further compared the changes in signaling pathways in the four treatment groups. We found that the activity of JAK-STAT, NFkB, TNFa, and PI3K signaling pathways progressively increased during disease progression, while the activity of Hypoxia progressively decreased. JAK-STAT, NFkB, and TNFa are typical inflammation-activated signaling pathways. The P53 signaling pathway was significantly reduced in the 2 days after VZV antigen challenge group.

The findings indicate that skin cells experience disruption in their cellular repair mechanisms following VZV antigen infection. Additionally, we observed a significant reduction in the TGFB signaling pathway in the group challenged with VZV antigen for 2 days. TGF-β is known to induce Foxp3-positive regulatory T cells (iTregs) in the presence of interleukin 2 (IL-2), while in the presence of IL-6, it leads to the generation of Th17 cells that produce pathogenic IL-17 (Xu et al. 2007). Furthermore, TGF-β hinders the proliferation of immune cells and cytokine production through both Foxp3-dependent and non-dependent mechanisms (Yoshimura and Muto 2010). JAK-STAT and NFκB signaling pathways are signaling pathways that are widely activated by immune cells during the natural immune response phase(Chen et al. 2018). In addition, we assessed the signaling pathway scores of the KEGG gene set in the four treatment groups using ssGSEA. We found that in the 6 h after VZV antigen challenge group, natural immune-related signaling pathways (NOD-like receptor signaling pathway, Toll-like receptor signaling pathway, RIG-I-like receptor signaling pathway) were significantly activated. This represents the early state of the immune response to VZV antigen stimulation of the skin. During the 2 days after VZV antigen challenge phase, both natural and active immunity were activated. It reflects the physiology of the skin in response to VZV antigen stimulation. Finally, we explored the process by which the cellular composition of the tissue microenvironment of the skin changed across the 4 treatment groups. We found that DC were significantly and positively correlated with Pseudo-time in all 4 treatment groups. The results suggest a major role for DC cell-mediated immunity (both natural and active) in the skin tissue during VZV antigen stimulation. Neutrophils were significantly positively correlated with Pseudo-time only in the 6 h after saline injection, 6 h after VZV antigen challenge group. The results suggest that neutrophils are mainly involved in the wound repair process(Diegelmann and Evans 2004). It has been shown that neutrophils are significantly aggregated at the wound site. Basal granulocytes, on the other hand, were significantly and positively correlated with Pseudo-time mainly in the VZV antigen-treated group. It is suggested that basal granulocytes play a major role in the repair of viral infections. Finally, a significant number of immune cells were activated in the 2 days after VZV antigen challenge group and were significantly positively correlated with Pseudo-time, whereas the opposite was true for stromal cells. It reflects the extensive immune activation and proliferation of skin tissue and apoptosis of stromal cells that occur in the late phase of the VZV antigen response.

In summary, this study has made full use of the transcriptomic information of the skin to explore the molecular biology and cell biology mechanisms of the stress response

process after VZV antigen stimulation of the skin, providing a theoretical basis for the development of VZV therapeutic drugs and vaccines. However, the conclusions obtained from this study need to be validated by further experiments.

Declarations

Competing interests The authors declare no competing interests.

References

Aran D, Hu Z, Butte AJ (2017) xCell: digitally portraying the tissue cellular heterogeneity landscape. Genome Biol 18:1–14

Arvin AM, Moffat JF, Sommer M, Oliver S, Che X, Vleck S, Zerboni L, Ku C-C (2010) Varicella-Zoster virus T cell tropism and the pathogenesis of skin infection. Varicella-zoster Virus 189–209

Badia-i-Mompel P, Vélez Santiago J, Braunger J, Geiss C, Dimitrov D, Müller-Dott S, Taus P, Dugourd A, Holland CH (2022) Ramirez Flores, decoupleR: ensemble of computational methods to infer biological activities from omics data. Bioinf Adv 2:vbac016

Balfour H Jr (1988) Varicella Zoster virus infections in immunocompromised hosts. A review of the natural history and management. Am J Med 85:68–73

Barrett T, Wilhite SE, Ledoux P, Evangelista C, Kim IF, Tomashevsky M, Marshall KA, Phillippy KH, Sherman PM, Holko M (2012) NCBI GEO: archive for functional genomics data sets—update. Nucleic Acids Res 41:D991–D995

Butler A, Hoffman P, Smibert P, Papalexi E, Satija R (2018) Integrating single-cell transcriptomic data across different conditions, technologies, and species. Nat Biotechnol 36:411–420

Chambers ES, Vukmanovic-Stejic M, Shih BB, Trahair H, Subramanian P, Devine OP, Glanville J, Gilroy D, Rustin MH, Freeman TC (2021) Recruitment of inflammatory monocytes by senescent fibroblasts inhibits antigen-specific tissue immunity during human aging. Nat Aging 1:101–113

Chen L, Deng H, Cui H, Fang J, Zuo Z, Deng J, Li Y, Wang X, Zhao L (2018) Inflammatory responses and inflammation-associated diseases in organs. Oncotarget 9:7204

Diegelmann RF, Evans MC (2004) Wound healing: an overview of acute, fibrotic and delayed healing. Front Biosci 9:283–289

G.O.C.J (2004) .N.a. research, the Gene Ontology (GO) database and informatics resource. Nucleic Acids Res 32:D258–D261

Gater A, Abetz-Webb L, Carroll S, Mannan A, Serpell M, Johnson R (2014) Burden of herpes zoster in the UK: findings from the zoster quality of life (ZQOL) study. BMC Infect Dis 14:1–14

Gershon AA, Gershon MD (2013) Pathogenesis and current approaches to control of varicella-zoster virus infections. Clin Microbiol Rev 26:728–743

Gershon AA, Gershon MD, Breuer J, Levin MJ, Oaklander AL, Griffiths PD (2010) Advances in the understanding of the pathogenesis and epidemiology of herpes zoster. J Clin Virol 48:S2–S7

Hafemeister C, Satija R (2019) Normalization and variance stabilization of single-cell RNA-seq data using regularized negative binomial regression. Genome Biol 20:1–15

Hänzelmann S, Castelo R, Guinney J (2013) GSVA: gene set variation analysis for microarray and RNA-seq data. BMC Bioinformatics 14:1–15

Holland CH, Tanevski J, Perales-Patón J, Gleixner J, Kumar MP, Mereu E, Joughin BA, Stegle O, Lauffenburger DA, Heyn H (2020) Robustness and applicability of transcription factor and pathway analysis tools on single-cell RNA-seq data. Genome Biol 21:1–19

Hyman R, Ecker J, Tenser R (1983) Varicella-Zoster virus RNA in human trigeminal ganglia. Lancet 322:814–816

Kanehisa M, Goto S (2000) KEGG: kyoto encyclopedia of genes and genomes. Nucleic Acids Res 28:27–30

Kassambara A, Kassambara MA (2020) Package 'ggpubr'. R package version 0.1 6

Langfelder P, Horvath S (2008) WGCNA: an R package for weighted correlation network analysis. BMC Bioinformatics 9:559

Liberzon A, Subramanian A, Pinchback R, Thorvaldsdóttir H, Tamayo P, Mesirov JP (2011) Molecular signatures database (MSigDB) 3.0. Bioinformatics 27:1739–1740

Oxman MN (2000) Clinical manifestations of herpes zoster. Varicella-zoster Virus: Virol Clin Manage 246:275

Perešíni P, Kuźniar M, Kostić D (2015) Monocle: Dynamic, fine-grained data plane monitoring, Proceedings of the 11th ACM Conference on Emerging Networking Experiments and Technologies, pp. 1–13

Reimand J, Isserlin R, Voisin V, Kucera M, Tannus-Lopes C, Rostamianfar A, Wadi L, Meyer M, Wong J, Xu C (2019) Pathway enrichment analysis and visualization of omics data using g: Profiler, GSEA, Cytoscape and EnrichmentMap. Nat Protoc 14:482–517

Revelle W, Revelle MW (2015) Package 'psych'. Compr R Archive Netw 337:338

Sadzot-Delvaux C, Merville-Louis M, Delree P, Marc P, Piette J, Moonen G, Rentier B (1990) An in vivo model of varicella-zoster virus latent infection of dorsal root ganglia. J Neurosci Res 26:83–89

Schellack N (2011) Skin rashes in children: evidence-based pharmacy practice. SA Pharm J 78:13–22

Schubert M, Klinger B, Klünemann M, Sieber A, Uhlitz F, Sauer S, Garnett MJ, Blüthgen N, Saez-Rodriguez J (2018) Perturbation-response genes reveal signaling footprints in cancer gene expression. Nat Commun 9:1–11

Stankus SJ, Dlugopolski M, Packer D (2000) Management of herpes zoster (shingles) and postherpetic neuralgia. Am Family Phys 61:2437

Sun J, Liu C, Peng R, Zhang F-K, Tong Z, Liu S, Shi Y, Zhao Z, Zeng W-B, Gao GF (2020) Cryo-EM structure of the varicella-zoster virus A-capsid. Nat Commun 11:1–11

Vafai A, Wroblewska Z, Wellish M, Green M, Gilden D (1984) Analysis of three late varicella-zoster virus proteins, a 125,000-molecular-weight protein and gp1 and gp3. J Virol 52:953–959

Wu T, Hu E, Xu S, Chen M, Guo P, Dai Z, Feng T, Zhou L, Tang W, Zhan L (2021) clusterProfiler 4.0: a universal enrichment tool for interpreting omics data. Innov 2:100141

Xu L, Kitani A, Fuss I, Strober W (2007) Cutting edge: regulatory T cells induce CD4 + CD25 – Foxp3 – T cells or are self-induced to become Th17 cells in the absence of exogenous TGF-β. J Immunol 178:6725–6729

Yamanishi K, Matsunaga Y, Ogino T, Takahashi M, Takamizawa A (1980) Virus replication and localization of varicella-zoster virus antigens in human embryonic fibroblast cells infected with cell-free virus. Infect Immun 28:536–541

Ye Z, Liu D, Liu D, Lv Y, Zhang Y, Zhang J, Bao J, Yuan X, Hou J, Li L (2022) Immune Infiltration of CD8 + T cells in patients with Diabetic Pancreatic Cancer reduces the malignancy of Cancer tissues: an in Silico Study. 12

Yoshimura A, Muto G (2010) TGF-β function in immune suppression. Negat co-receptors Ligands 127–147

You Y, Cheng A-C, Wang M-S, Jia R-Y, Sun K-F, Yang Q, Wu Y, Zhu D, Chen S, Liu M-F (2017) The suppression of apoptosis by α-herpesvirus. Cell Death Dis 8:e2749–e2749